Mode-Selective MIMO OTH Radar: Demonstration of Transmit Mode-Selectivity on a One-Way Skywave Propagation Path

G. J. Frazer*, Y. I. Abramovich*, and B. A. Johnson‡
*ISR Division, DSTO, Edinburgh, SA, AUSTRALIA
gordon.frazer@dsto.defence.gov.au
‡LM Australia Electronic Systems Pty. Ltd. Edinburgh, SA, AUSTRALIA

***Abstract*— This paper reports results of an experimental program called the Mode Selection Experiment that was designed to demonstrate ionospheric mode selectivity on transmit over a one-way skywave propagation path. This corresponds to the transmitter-to-target part of the two-way propagation path used in an Over-the-Horizon Radar. The purpose of the experiment was to show that multiple-input multiple-output radar techniques can be used to construct the required multiple simultaneous adaptive range-dependent transmitter beams needed in a Mode-Selective Over-the-Horizon Radar, which is a new class of skywave radar designed for Maritime Domain Awareness applications. The results comprehensively show that a beam can be created and applied to selectively illuminate desirable ionospheric propagation paths while simultaneously nulling undesirable propagation paths. It is possible to simultaneously create a different such beam for each range cell in the range coverage and so achieve mode-selectivity throughout the full range extent of the radar.**

***Index Terms*— HF radar, over-the-horizon radar, MIMO radar, adaptive radar transmitter, skywave, mode selectivity**

I. Introduction

The paper presents experimental results demonstrating ionospheric propagation mode selectivity on transmit in a form relevant for skywave Over-the-Horizon Radar (OTHR) [1]. This is an important step in the development of Mode-Selective Over-the-Horizon Radar, which is a recently introduced concept that has the potential to significantly improve the performance of skywave OTHR against slow moving targets such as maritime vessels [2]. Mode-Selective OTHR is a radar architecture that is designed to enhance the performance of skywave radar against maritime targets during periods of disturbed or multi-mode ionospheric propagation conditions. It achieves this using spatial selectivity in both azimuth and elevation, on both transmit and receive, and uses this joint transmit-receive 2D selectivity in azimuth and elevation as the basis of a strategy for minimising spread-Doppler clutter and multi-mode contamination of target radar returns [2]–[7].

With Mode-Selective OTHR a crucial requirement is the ability to form range-dependent adaptive propagation-mode selection beams for the transmitted radar signal. This requirement exists for the target-to-receiver path as well. However, this capacity has been established previously using 2D receive apertures e.g. see [8] although, for completeness, later in the paper we present results for mode-selectivity on receive to show the duality with the transmit case. The design of transmit and receive apertures with appropriate joint properties remains a question of interest and will be discussed elsewhere. The aforementioned transmitter beams need to be non-causal and adaptive, to counter the unknown and time-varying behaviour of the dynamic ionosphere, and need to be range dependent, since there will be a different beam pattern required for each range cell, based on the propagation geometry from radar to target region of interest. For the geometry of OTHR, propagation via the ionosphere introduces dependence between elevation direction-of-departure from the transmitter, target range, and elevation direction-of-arrival at the radar receiver.

Here the term "non-causal" is used to express that the transmit beamforming that is traditionally applied at the transmitter *prior* to signal radiation ("causal" beamforming) is now applied at the receiver *after* signal transmission, propagation, scatter, propagation and reception (for the two-way case). In the non-causal approach, both transmit and receive beamforming is applied at the receiver post signal propagation. We appreciate that causality is not in fact broken but use the term to reinforce that the traditional perception of transmit beamforming actually forming a beam at the transmitter and then propagating from the transmitter does not apply in our approach.

The experimental results in this paper extend our previous work and demonstrate transmit adaptive non-causal *ionospheric propagation-mode selectivity* over a realistic one-way ionospheric propagation path. Previously we had investigated this class of beamforming in the azimuth and elevation cases separately, where in the latter case we used an unrealistically limited aperture. In this paper, we take a further step and show mode separability in elevation over a realistic one-way transmitter-to-target propagation path using a multiple-input single-output (MISO) configuration with a local end-fire transmitter array of appropriate resolution and several widely dispersed single channel receiver systems located down-range.

A. Prior and Related Work

Previous work by the authors [2], [4], [6], [7], [9]–[12], and the references therein, has addressed a range of issues relevant to designing a Mode-Selective OTHR. Taken together, the results thus far have comprehensively demonstrated that

multiple-input multiple-output (MIMO) radar techniques work in the HF radar context and are a key enabler for the clutter mitigation strategy adopted in the Mode-Selective OTHR approach. Keep in mind that there are other radar design issues as well for the Mode-Selective OTHR. This type of radar requires more innovation that MIMO alone. This paper is concerned only with experimental results demonstrating mode-selectivity on transmit with the remaining Mode-Selective OTHR matters to be discussed elsewhere.

The field of bi-static and multi-static radar and the newer use of MIMO techniques in these configurations is well described in an extensive collection of established and recent literature [1], [13]–[21] and the references therein. Initial MIMO radar material appeared in [22]–[26]. The relationship of [24], which uses the established language of the sum and difference co-array, to MIMO radar, is discussed in [9].

Of particular relevance to the work reported here are examples of experimental MIMO systems. In addition to our own work (see the references above) there have been a number of demonstrations that explore the applicability of MIMO in radar. The original concept of spatially coding the transmitted signal was reported in 1989 [22] with experimental results given in [23]. The remarkable RIAS is the first known MIMO radar.

The earliest reported experimental use of MIMO since RIAS is the work on distributed apertures by Robey and Coutts and their co-authors in 2004 at MIT Lincoln Laboratory [27], [28]. They demonstrated coherent radar action across multiple distributed apertures using MIMO radar concepts. They used multiple line-of-sight radars operating at X-band. More recently the same group has been applying MIMO to OTHR although little has appeared in the literature [29], [30].

Experimental results showing the use of MIMO techniques to enhance performance in airborne radar applied to ground moving target indication (GMTI) is reported by Kantor, Davis and Bliss, also of MIT Lincoln Laboratory, in [31], [32]. While unrelated to OTHR the results described in their work make a compelling case for MIMO use in airborne GMTI radar.

Krolik, Mecca and Yu at Duke University have reported MIMO experimentation using both radar and acoustic systems at low-power in the laboratory [33], [34]. The same group have also published theoretical and algorithm investigations concerning OTHR applications of MIMO techniques [35] (and the references therein).

In an application similar to our own interest concerning clutter mitigation in HF radar Riddolls and co-authors at Defence Research and Development Canada detail an experimental investigation into the use of MIMO techniques for the mitigation of Auroral clutter for a proposed northern looking skywave OTHR based in Canada [36], [37]. These are initial results and part of an on-going investigation and further results are anticipated over the next few years.

II. Paper Outline

The purpose of the paper is to report experimental results showing mode-selectivity on a one-way ionospheric propagation path. Prior and related work is discussed in section I. In section III the concept of a skywave Mode-Selective OTHR is discussed. The goal of this new class of OTHR is to increase the period of total operating time for which ionospheric propagation conditions can support effective detection and tracking of slow moving vessels. We introduce our notation and detail the signal model employed and outline the analysis applied to the measured data in section IV. The experiment is described in detail in section V and which includes some information about the ionospheric sounding system we installed for the period of the data collection in order to provide accurate insight into ionospheric conditions throughout the experiment. The key results and corresponding analysis are reported in section VI. We finish with our lessons learned and concluding remarks in section VII.

III. Mode Selective OTHR

Current generation skywave over-the-horizon radars (OTHR) possess significant but limited wide-area maritime surveillance capability [1], [38], [39]. These radars are typically operated in concert with a range of other maritime surveillance assets to generate a maritime surveillance picture and hence contribute to national-level maritime domain awareness (MDA). The other surveillance assets are generally complementary to OTHR and include; civilian and military manned and unmanned maritime patrol aircraft (MPA), maritime patrol surface vessels, shore-based microwave radar, high frequency surface-wave radar (HFSWR), cooperative systems such as Automatic Identification System (AIS) or Long Range Identification and Tracking and various procedural position reporting systems. No single sensor modality provides the complete sensor solution. Persistent MDA requires that the data from many or all of these sensors be combined in an appropriate manner.

Unsurprisingly, each of these sensor systems has their own capability strengths and weaknesses; for example, AIS provides highly accurate target location information, and includes target identification, but is cooperative, and so relies on "good citizen" behaviour, and hence is unlikely to be available for hostile surface vessels. Maritime patrol aircraft (MPA) have long been recognised as effective maritime surveillance systems. They provide an identification capability in addition to target detection and tracking - at least for the loiter period of the aircraft - provided they have actually found the target in the first instance. Their disadvantage is that they are expensive to procure, operate and support. They are best used with appropriate cueing, whereby other sensors or information is used to provide the MPA mission planners with advice as to likely target locations and hence allow them to develop resource efficient mission routes. OTHR, on the other hand, is an excellent complement. It can provide the detection and tracking elements of maritime surveillance at extended distance from the coast and over wide areas of open ocean. It is relatively low-cost on a per square kilometer of surveillance area covered basis (relative costs for the air surveillance case has been estimated in [37]).

Perhaps the two most important of these limitations is that OTHR cannot provide target identification and that performance is highly variable with changing ionospheric conditions

and in particular performance deteriorates during periods of spread-Doppler ionospheric propagation, or multi-mode ionospheric propagation, or both.

When seeking slow-moving surface vessels, current generation OTHR systems lack a comprehensive means of removing spread-Doppler and multi-path propagation, and hence are subject to *reduced* and *uncertain* performance during periods of typical ionospheric propagation variation. Current radars also are subject to reduced performance in high sea-state and the absolute geo-location accuracy of OTHR can be poor at times. This latter issue results from uncertain operator knowledge of ionospheric multi-path propagation. Improving both the performance of, and the certainty with which, maritime vessel detection and tracking can be achieved has long been a research challenge within the OTHR community.

Typically OTHR are designed for surveillance of aircraft with the surface vessel problem as an adjunct mission, where in the latter case, the radar is subject to the limitations discussed in the previous paragraph.

In [2] we proposed a new OTHR design that is directed primarily at MDA, with air target capability as the adjunct mission. Since it primarily exploits mode selectivity we named this new skywave radar *Mode-Selective OTHR* and we use this term throughout the paper to mean a skywave radar with an appropriate architecture that can exploit propagation mode selection/rejection to enhance target detection and tracking performance.

A. Ionospheric Propagation Geometries

The core idea is an OTHR architecture designed specifically to exploit the "best" ionospheric propagation mode or modes, while simultaneously minimising propagation and hence contamination by other ionospheric propagation modes, including the frequently Doppler-disturbed F-mode propagation often used for long-range aircraft surveillance. There may be more than one single suitable propagation mode and in the architecture proposed it is possible to isolate individual suitable propagation modes and hence provide *mode-diverse* measurements of the target area of interest.

OTHR achieves beyond line-of-sight horizon target detection and tracking by exploiting radiowave propagation via the ionosphere. Davies [40] describes the ionosphere as that part of the upper atmosphere where sufficient ionisation can exist to effect the propagation of radio waves. The peak electron density usually occurs in the F region (140km and above) which is sub-divided into the F_1 layer (typically centered on 200km) and the F_2 layer (typically centered on 300km). Below the F region is the E region (90km to about 140km). The E region contains the normal E layer as well as areas of atypical electron concentration referred to as "sporadic E" or E_S. The differing effective region heights mean that radiowaves propagating via the ionosphere to the earth surface with similar delay or (radar) range will depart the transmitter and arrive at the receiver at differing elevation angles. The structures and peak densities in the ionosphere vary greatly with time, with geographical location and with certain solar disturbances [40].

In the OTHR target detection case, depending on the particular ionospheric conditions, there may be several propagation paths or modes from the transmitter to the target and earth surface and return from the target and earth surface to the receiver. For example, in the case of both E and F region propagation support, there can be four paths (with the same radar range) from transmitter to target/earth surface (or clutter source, such as the ocean surface) to receiver: denote as E-E the transmitter to target on E mode and target to receiver on E mode case, and then E-F, F-E and F-F are the remaining three paths defined similarly (although in these cases scattering is from the earth surface at the same radar range but at different ground range from the radar). Other less geometrically obvious modes are also possible (e.g. E-F_1, F_2-F_1, $F_{2\ \mathrm{Low}}$-$F_{2\ \mathrm{High}}$ and so forth). The diagram in figure 1 shows two ionospherically propagated paths with the same radar range (i.e. same time delay) where one path propagates via the E layer and one via the F layer. The take-off elevation angle for each path is different. Note that the location on the earth surface is different for each propagation path.

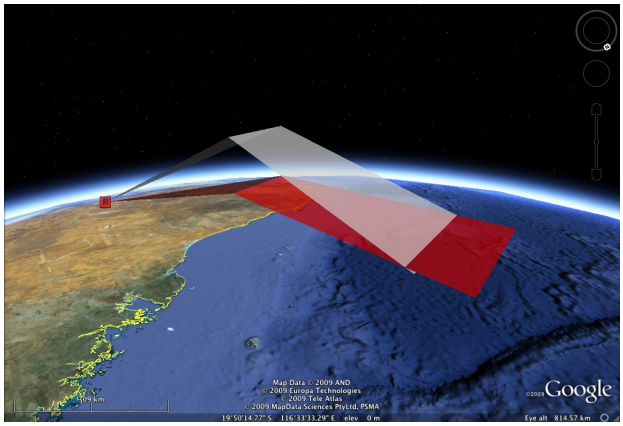

Fig. 1. Two ionospherically propagated paths with the same radar range but where each path propagates via a different layer in the ionosphere. Note the different take-off elevation angles for each propagation path at the radar location. For a particular radar range, the location of scatter from the ground is different for the two modes.

B. Concept

Surface vessels are slow moving compared with aircraft. Therefore, coherent integration intervals exceeding ten seconds are required to successfully isolate surface targets from ocean clutter. Temporal and spatial variations in the ionosphere can exist on time-scales less than the coherent integration interval of the radar. In these cases the Earth return clutter will be corrupted by the time-varying propagation path leading to a phenomenon known as spread-Doppler clutter. In certain circumstances this can obscure targets and be a severe impediment to target detection and track initiation and sustainment. Dynamic ionospheric behaviour causing spread-Doppler clutter largely affects the F region but almost never affects the E region. See the examples in [41] for an indication of the deleterious impact of spread-Doppler clutter due to propagation via a disturbed F layer as well as a case of excellent propagation support for surface vessel detection

via E layer propagation. In some circumstances multi-mode propagation will exist where each mode in isolation will be suitable for maritime vessel detection and tracking but the composite of all modes present without discrimination will render poor detection performance.

The concept of a Mode-Selective OTHR is to reject by some technical means the propagation modes that are corrupted by spread-Doppler clutter or multi-mode propagation. The radar is designed to permit effective elevation filtering at both the transmitter and the receiver in the general case of a bi-static radar and for the example presented earlier to retain support for elevation angles that propagate via the E region and reject propagation via elevation angles that are supported via the F region. Such spatial elevation filtering is required on both the transmitter-to-target and the target-to-receiver propagation paths to mitigate the F-F and mixed E-F and F-E propagation modes. Such filtering must be different for each *range-of-interest* since in OTHR radar range is coupled with transmit signal take-off elevation and the elevation of signal arrival at the receiver. Full spread-Doppler clutter mitigation therefore must be implemented on both the transmitted signal and the received signal jointly and with a different solution for each range in the radar range gate. Due to the time-varying behaviour of the ionosphere, the filtering discussed also needs to be time-varying to adapt to the dynamic ionosphere.

Figures 2 and 3 show ray-tracing through a typical ionosphere for E-layer propagation to 1800km ground range. Figure 2 shows the case of 1800km ground range and all possible E-$F_{2\ \mathrm{Low}}$ and E-$F_{2\ \mathrm{High}}$ modes with the same total radar range as E-E propagation. Figure 3 shows the cases for all F layer propagation for which the two-way radar range is the same as the two-way E layer propagation radar range. Elevation angles vary from 2.99^o to 24.56^o. A radar architecture that filters in elevation on *both* transmit and receive requires elevation discrimination for angles preserved at 2.99^o and rejected at or greater than 15.73^o while the corresponding case of filtering on *either* (but not both) transmit or receive requires elevation discrimination for angles preserved at 2.99^o and rejected at 3.49^o. The aperture resolution requirements in this latter transmit or receive only case are demanding, and, particularly for an earth-conformal aperture, are likely unobtainable in a practical OTHR design. Even in the former case it is expected that the array depth of the transmit and receive arrays will need to be approximately 1200m or greater for the case of an earth-conformal arrays.

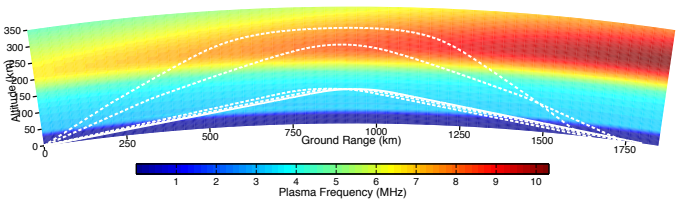

Fig. 2. Ray-trace paths for the case of propagation to 1800km ground range and all possible E-$F_{2\ \mathrm{Low}}$ and E-$F_{2\ \mathrm{High}}$ modes with the same total radar range as E-E propagation. Elevation angles vary from 2.99^o to 24.56^o.

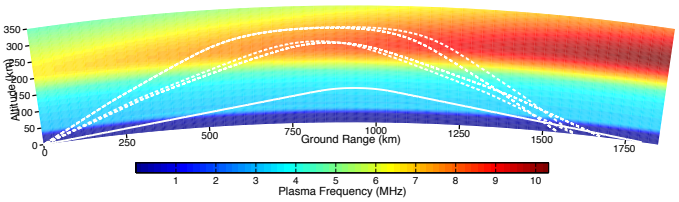

Fig. 3. Ray-trace paths for the case of propagation to 1800km ground range and all possible F layer modes with the same total radar range as E-E propagation. Elevation angles vary from 2.99^o to 24.54^o.

C. Architecture

Mode-Selective OTHR has four specific radar architecture features that differ from a conventional second generation operational OTHR such as JORN [42], [43]. These are:

1) directivity in both azimuth and elevation on both transmit and receive including the ability to form range-dependent adaptive and non-causal transmit and range-dependent adaptive receive beams
2) earth conformal planar two-dimensional transmit and receive antenna array systems that are operating with extreme steer angle (with respect to boresight)
3) reduced transmitter power since target detection will almost always be a target-in-clutter detection problem as compared to the target-in-noise case
4) automatic tracking algorithms designed to sustain tracks through substantial periods without new measurements

We note that sensor management will differ as compared with conventional OTHR but that clear-channel advice, background noise monitoring, backscatter power and channel Doppler assessment functions will still be required. Total system cost is reduced compared with second generation OTHR since high power transmitting systems are not needed. Transmit power can be reduced since for the detection in clutter problem there is no loss of sensitivity for reduced power on transmit provided the detection problem remains one of target detection in clutter. At some point transmit power will be reduced to such a degree that the detection problem reverts to detection-in-noise. A Mode-Selective OTHR is expected to have adjustable transmit power levels greater than this lower limit.

Of the four features listed, it has hitherto been the lack of the first two (range-dependent adaptive transmit beamforming, and, a 2-D transmit antenna array operating with extreme steer angle) that has previously inhibited the concept of a Mode-Selective OTHR.

D. Operational Issues and Comments

A Mode-Selective OTHR will have a different concept of operations compared to conventional OTHR employed for air target surveillance. Firstly, operational advice algorithms designed to optimise performance will differ. For example, carrier frequency selection will now need to include consideration of mode-separability in addition to the standard frequency selection considerations. Secondly, since the radar is unlikely to sustain 24 hour operations, either a period of no surveillance should be acceptable or alternative provision made to sustain surveillance during any period where there

is insufficient propagation support. For example, assuming E-mode propagation, a typical ocean-going vessel can be expected to travel less than 400km overnight during the period of no propagation support. This distance is substantially less than the total range and azimuth extent of the radar. The predictability of the propagation outage means that other MDA surveillance assets, such as MPA, can be applied in a predictable manner to sustain the maritime surveillance picture during this period. For example, it may be that a MPA fleet is allocated the task of visually identifying all maritime vessels detected and tracked by the Mode-Selective OTHR during the previous 12 hour period of radar measurement. This means the target identification capability of the MPA fleet will be employed without the need for flying time to conduct undirected new-target search and flying hours can be scheduled well in advance. Alternatively, the radar tracker may be set to sustain dead-reckon tracks between radar measurements including during the extended 12 hour measurement outage, or, include other sources of surface vessel location reports, such as those reporting cooperatively using AIS.

IV. Notation, Signal Model and Processing

The MISO based transmitter scheme that we use in the work reported in the paper consists of K transmitter antenna array elements concurrently transmitting K different radar waveforms $\mathbf{u}(t) = u_1(t), \ldots, u_k(t), \ldots, u_K(t)$ of equal energy. This is the element-space waveform set case where there is a one-to-one mapping between waveforms and array elements. Other configurations such as beam-space, which map one waveform per beam in a multi-beam arrangement, and sub-array space, which map one waveform per antenna sub-array, were not used in the experiment and so are not considered here.

A single radar receiver is located to receive the propagated waveform set.

$$Z(t) = \eta_0 \sum_{k=1}^{K} a_k(\theta_d) u_k(t - \tau_0) \mathrm{e}^{j2\pi\nu_0 t} \tag{1}$$

where η_0 is a random complex scattering coefficient that is assumed identical for all waveforms, τ_0 and ν_0 are the delay and Doppler shift of the one-way propagation channel, and,

$$\mathbf{a}_K(\theta_d) \equiv [a_1(\theta_d), \ldots, a_K(\theta_d)]^T \tag{2}$$

is the K-variate transmit antenna array manifold (steering) vector for the direction-of-departure θ_d that will illuminate the propagation path.

The received radar return $Z(t)$ is processed as for conventional radar receive processing (matched filter, etc) K times, once for each waveform in the waveform set as the reference waveform. Let $\mathbf{z}(\nu, \tau) = z_1(\nu, \tau), \ldots, z_k(\nu, \tau), \ldots, z_K(\nu, \tau)$ be the outputs of the K respective discrete-time matched filters indexed in Doppler ν and delay (or equivalently range) τ and extending over the domain S of anticipated scatterer extent $S \in (\nu, \tau)$. The transmitter beamformer is then

$$y(\nu, \tau) = \mathbf{w}^H \mathbf{z}(\nu, \tau) \tag{3}$$

for some beamformer weight $\mathbf{w}$. We seek to investigate how we can create various $\mathbf{w}$ to demonstrate the mode-selectivity aspect of Mode-Selective OTHR.

The particular waveform set should be selected such that the cross-ambiguity between the K members of the waveform set does not adversely interact with the expected target and clutter scatterer distribution in delay and Doppler. This means choosing (for the discrete-time representation of $\mathbf{u}(t)$ assumed in our radar signal processing and with $j = \sqrt{-1}$ in this equation)

$$\chi_{k,l}(\nu, \tau) = \sum_{S} u_k(t) * u_l^*(t - \tau) \mathrm{e}^{-j2\pi t\nu} < \epsilon \text{ for } k \neq l \tag{4}$$

over the domain of Doppler-delay space S that one anticipates scatterer response to be present and ϵ is some small value that specifies the upper acceptable limit of cross-ambiguity between waveforms. See the full discussion in [7] and the experimental examples in [11] which includes an example where there is significant cross-coupling between scatterer responses from different members of the waveform set.

A. Adaptive Mode Selection

The adaptive spatial processor used is the well-known minimum variance distortionless response (MVDR) beamformer [44]. The MVDR beamformer is defined for a preserved steer direction θ as

$$\mathbf{w}_o = \frac{R^{-1}\mathbf{s}(\theta)}{\mathbf{s}^H(\theta) R^{-1} \mathbf{s}(\theta)} \tag{5}$$

where

$$\mathbf{s}(\theta) = [1, \mathrm{e}^{j\theta}, \ldots, \mathrm{e}^{j(K-1)\theta}]^T \tag{6}$$

This choice of $\mathbf{w}_o$ ensures that total beamformer output energy $|\mathbf{w}_o^H R \, \mathbf{w}_o|$ is minimised while the preserved steer direction gain $\mathbf{w}_o^H \mathbf{s}(\theta) = 1$. In practice, the covariance matrix R is estimated from a region of Doppler-delay space comprising P Doppler cells by Q delay cells. The sample covariance matrix is given by

$$\hat{R} = \frac{1}{PQ} \sum_{i=1}^{P} \sum_{j=1}^{Q} \mathbf{z}(\nu, \tau) \mathbf{z}^H(\nu, \tau) \tag{7}$$

This estimated covariance matrix $\hat{R}$ is used in place of the exact covariance R in equation (5). Reduction of achieved signal to noise ratio improvement using the beamformer due to the use of $\hat{R}$ in place of R is discussed in the established work of [45].

Throughout the paper we use the term *MVDR mode-selective beamformer* to indicate the use of the algorithm detailed in this section. In all cases we select $\mathbf{s}(\theta)$ from either an estimate (for example, from equation (8)) of a desired θ and knowledge of the array manifold determined using an off-line calibration procedure, or, alternative, select $\mathbf{s}(\nu, \tau)$ as a desirable feature in range-Doppler space to preserve. While the latter lacks a physical interpretation of direction-of-departure it is useful in cases where the array manifold calibration solution is unavailable. Training data is selected according to equation (7) where the domain of range-Doppler space included is chosen to capture the signal energy we seek

to remove. Equation (5) is then solved and the beamformer applied as in equation (3) over the range-Doppler domain (ν, τ) of interest.

B. Direction-of-Departure Estimation

The estimated direction-of-departure (DOD) $\hat{\theta}^d(\nu, \tau)$ from the transmitter array for a signal propagating from that array to a down-range receiver via the ionosphere and corresponding to the signal at Doppler-delay cell (ν, τ), is given by

$$\hat{\theta}^d(\nu, \tau) = \max \arg_\theta |y(\nu, \tau, \theta)|^2 \quad (8)$$

A full beampattern for the energy in Doppler-delay cell (ν, τ) can be determined by evaluating $|y(\nu, \tau, \theta)|^2$ for all θ of interest. Note that the DOD measured from a linear one-dimensional array in a two-dimensional environment is the so-called cone angle with respect to array axis (or end-fire). The cone angle is a coupled measurement of azimuth and elevation where these latter two parameters are with respect to a plane containing the linear array and one other reference direction. In our case it is the plane of the earth containing the array. In the following we exploit exact knowledge of the azimuth from transmitter to receiver to determine elevation-of-departure θ^e from direction-of-departure θ^d according to

$$\theta^e = \cos^{-1}[\frac{\cos \theta^d}{\cos \theta^a}] \quad (9)$$

where θ^a is our a-priori knowledge of the bearing from the transmitter array to the down-range receiver adjusted for coordinate system.

V. Experiment Description

The Mode Selection Experiment (MSE) reported here took place during December of 2009 (MSE-I) and March of 2010 (MSE-II) in central and northern Australia. To provide some context for these campaigns the geographic layout for the December 2009 experiment is shown in Fig. 4. In both MSE-I and MSE-II the transmitter array and MISO transmission equipment and the experiment central control were located at Coondambo in South Australia. This site also had a wide-band oblique incidence sounder (OIS) transmitter [46] to support propagation assessment, and a clear-channel advice system for operating frequency selection.

In the December 2009 MSE-I campaign three single channel radar receivers were deployed down-range at various propagation distances with similar aspect. Receiver systems were placed at Mt Everard (863km at a bearing of 345.0^{o}T - defined with respect to the Coondambo transmit site and clockwise relative to true North), Elliott (1514km at a bearing of 350.5^{o}T) and at Tindal (1864km at a bearing of 348.2^{o}T). In March 2010 we added a further two single channel radar receivers, one at Hermannsburg (844.4km at a bearing of 338.2^{o}T) and one at Kings Canyon (867.2km at a bearing of 329.4^{o}T). For MSE-II we also converted all receiver systems to be capable of real-time MISO processing. Locations were selected to provide diversity in range (MSE-I) and range and bearing (MSE-II). All down-range receiver systems operated synchronously with the transmit system. Mode selection solutions generated for one location could simultaneously be assessed for mode rejectability at the various different ranges and bearings with respect to the transmitter. Range and bearings for all five down-range sites are summarised in table I.

Location	Range (km)	Bearing (^{o}T)	Azimuth (^{o})
Mt Everard	863.0	345.0	-14.5
Elliott	1514.0	350.5	-9.0
Tindal	1864.0	348.2	-11.3
Kings Canyon	867.2	329.4	-30.1
Hermannsburg	844.4	338.2	-21.3
Glendambo	15.8	313.2	-46.3

TABLE I

TABLE OF RANGE, BEARING AND AZIMUTH WITH RESPECT TO THE TX ARRAY LOCATION (BORESIGHT 359.5^{o}T).

In a preamble to MSE-II we placed radar receivers on the elements of the Coondambo transmit array and placed a radar transmitter at the Elliott site to gather comparative single-input multiple-output (SIMO) data to reproduce the previously demonstrated mode selectivity on receive that is relevant for the target to receiver path in the two-way sky-wave OTHR scenario. We also placed a broadband repeater transponder at a third location approximately 10km from the Kings Canyon receiver site to support some preliminary two-way point-scatterer backscatter investigations conducted at the end of MSE-II. An additional receiver site was established at Glendambo approximately 16km from the Coondambo transmit location at a respective azimuth very different than the respective azimuth to all other down-range receiver sites. With this system it was possible to measure point scatterer backscatter - two-way - radar returns from the transponder for the path: Coondambo transmitter to Kings Canyon transponder to Glendambo receiver.

In all MISO cases the down-range systems were unattended and operated remotely from the central control site at Coondambo. Each receiver location recorded and processed both the transmitted MISO waveform set as well as the wide-band oblique incidence sounder (OIS) transmission which provided information concerning the prevailing ionospheric propagation conditions between the transmitter location and the down-range locations. The OIS measurements also allowed an independent measure of the take-off elevation angles for the various propagation modes and paths involved as a check for the elevation directions-of-departure determined from the MISO transmit array.

Each down-range radar receiver incorporated computing, control and communications equipment designed to provide local processing, remote control and display. The control and display was remoted back to the central control location at the Coondambo transmit facility. We used both satellite and 3G cell-phone systems for the communications links. Local-to-the-receiver processing was operated via the remote control data links permitting real-time non-causal adaptive beamforming to be applied to the received data which we were able to observe in real-time at the central control location. The performance of our mode selectivity approach at all down-range sites could be viewed simultaneously. Transmit beamformer solutions generated at the receiver sites could be

Fig. 4. Geographic layout for MSE-I shown on the map of Australia. The experiment used equipment located at Coondambo (Tx array, OIS Tx and clear channel advice receiver), and receiver systems located at Mt Everard (863km), Elliott (1514km) and Tindal (1864km). The total ground-range depth between the nearest and furthermost receiver system is approximately 1000km and all receiver locations have similar orientation with respect to the transmitter array. Precise range, bearing and azimuth details for both campaigns are given in table I.

fixed and held for subsequent received coherent measurement intervals in order to assess temporal stability. These solutions could be fed back to the transmitter system and applied as a conventional transmit beamformer to compare the energy budget between MISO and conventional single-input single-output (SISO) transmit beamforming. Mode selection beamformer solutions determined at one location could not be applied to other down-range locations in real-time but this comparative analysis was undertaken post experiment.

The waveform set used comprised M_t=12 time-staggered linear frequency modulated continuous wave (LFMCW) waveforms, where the individual waveform set member start-time was uniformly dispersed in time throughout the waveform repetition interval. The choice of waveform set cardinality is based on the results reported in [7], [11]. A spectrogram of the radiated waveform set received at Mt Everard is shown in Fig. 5 where the time-staggered waveform set can be clearly recognised. For comparison a spectrogram of a conventional single LFMCW waveform transmitted from Elliott and received at Coondambo during the MSE-II preamble receiver array test is shown in Fig. 6.

The transmitter array at Coondambo comprised a 12 element minimum redundancy array with a total aperture of 1200m (end-fire bearing 359.5^{o}T). The array geometry is configured to provide elevation discrimination in the direction of the receiver locations. This aperture corresponded to our estimate of the likely spatial resolution required for effective mode selection in elevation. The minimum redundancy elemental unit spacing was $\{1, 2, 3, 7, 7, 7, 7, 7, 4, 4, 1\}$ spanning 50 units with a unit element spacing of 24m. The transmitter system could transmit up to 100W power per element and the array is shown in Fig. 7. In this experiment we used element-space MISO where each member of the waveform set (cardinality M_t=12) was transmitted via a separate element in the transmit array. Separate antennas were provided for OIS transmission and for a receiver to allow operating frequency selection advice. The array is designed to operate over a frequency range of 8-12MHz which was the anticipated range of ionospheric propagation support for the chosen down-range receiver locations during December 2009 and March 2010 (noting that ionospheric propagation conditions changed slightly during the three month interval between the experimental campaigns).

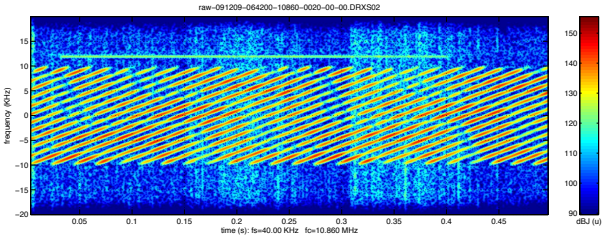

Fig. 5. Spectrogram showing time-frequency representation of the radiated waveform set as recorded at the down-range receiver located at Mt Everard. The waveform parameters were f_b=20KHz, f_{wrf}=4Hz and M_t=12. The units are time (s) on the horizontal axis and frequency (KHz) on the vertical axis.

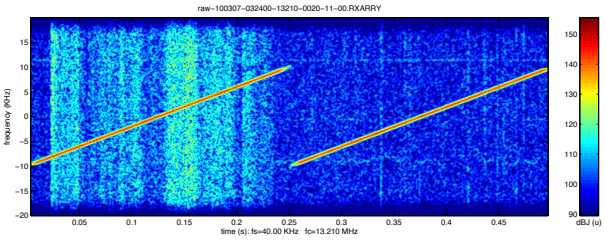

Fig. 6. Spectrogram showing time-frequency representation of a single LFMCW waveform. Compare this traditional radar transmission with the MISO waveform set in Fig. 5. The waveform parameters were f_b=20KHz, f_{wrf}=4Hz and M_t=1. The units are time (s) on the horizontal axis and frequency (KHz) on the vertical axis.

VI. Results

A. Mode Selectivity on Transmit

A snapshot of typical results demonstrating mode selectivity on transmit are shown in Fig. 8 and Fig. 9. The receiver data comprising range-Doppler maps for the 12 TX channel waveforms is shown in Fig. 8 for one example coherent processing interval of data recorded at Mt Everard. Four propagation modes are clearly observed for each waveform. The four modes have been identified from the accompanying OIS ionogram record to be 1E (one-hop propagation via E-layer), $1F_{2l}$ (one-hop propagation via F_2-layer low-ray), $1F_{2h\text{-}o}$ (one-hop propagation via F_2-layer ordinary high-ray) and $1F_{2h\text{-}x}$ (one-hop propagation via F_2-layer extraordinary high-ray) [40]. It is the adaptive weighted combination of the resolution cells across these 12 range-Doppler maps that allows mode-selectivity by non-causal transmit beamforming on receive.

We present two examples of mode selectivity in Figure Fig. 9. In the first example we have selected the $1F_{2h\text{-}o}$ (third mode out in range) to preserve and our goal is to reject all

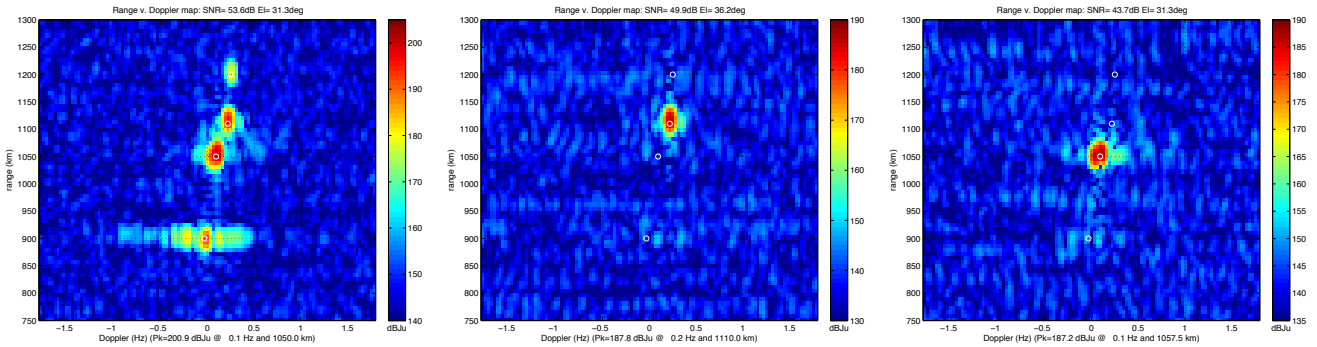

(a) Single Channel Response showing four modes (b) Preserve $1F_{2h\text{-}o}$ mode, Reject others (c) Preserve $1F_{2l}$ mode, Reject others

Fig. 9. A series of range-Doppler maps show the effect of the adaptive transmitter processing for different mode selection. The first subfigure corresponds to a single waveform channel. This is the response expected for a conventional OTHR measured over a one-way propagation path, and shows four modes which have been separately identified as (from minimum to maximum range) 1E, $1F_{2l}$, $1F_{2h\text{-}o}$ and $1F_{2h\text{-}x}$. The second and third subfigures are range-Doppler maps computed for this dataset using weight vectors determined using the MVDR algorithm, but with different preserved modes. In both cases, the unwanted modes have been rejected to the noise floor. All these cases can be computed simultaneously using the same received data, enabled by the non-causal MIMO transmit beamforming architecture. In all three cases, the peaks of the four propagation modes are marked with white circles, the units are Doppler (Hz) on the horizontal axis and radar range (km) on the vertical axis, and the intensity units dBJu are dB Joules uncalibrated.

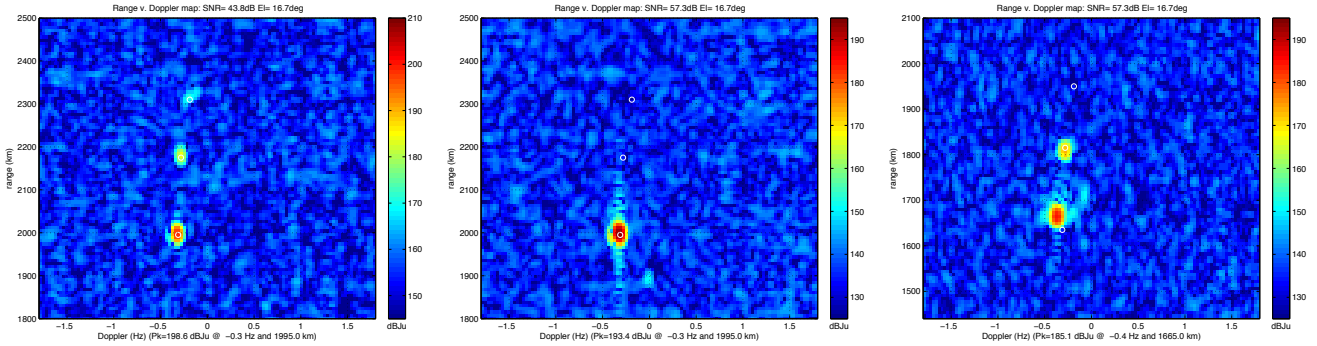

(a) Single Channel Response showing three modes (b) Preserve $1F_{2l}$ mode from Tindal (c) Use Tindal MVDR weights at Elliott

Fig. 10. A series of range-Doppler maps show the effect of the adaptive transmitter processing for different ranges. The first subfigure corresponds to a single waveform channel showing the mode structure measured at Tindal (range 1864km). The modes here (from minimum range to maximum range) have been identified as $1F_{2l}$, $1F_{2h\text{-}o}$ and $1F_{2h\text{-}x}$. This range is too long to allow for 1E propagation. The second subfigure is the range-Doppler map showing the mode-selection/rejection beamformer determined using and applied to the Tindal data (range 1864km). The third subfigure is the range-Doppler map showing the mode-selection/rejection beamformer determined using the Tindal data but then applied to the simultaneously recorded Elliott data (range 1514km). Note the poor mode rejection of the second-in-range mode. In all three cases, the units are Doppler (Hz) on the horizontal axis and radar range (km) on the vertical axis, and the intensity units dBJu are dB Joules uncalibrated.

other propagation modes. In Fig. 9(b) we see that all three unwanted modes have been rejected to the level of the noise floor using the MVDR mode-selective beamformer. In the second example shown in Fig. 9(c), the $1F_{2l}$ mode (second mode out in range) is preserved while the remaining modes are rejected. The rejection performance of the two examples is comparable and we stress that isolating these two modes individually on the basis of differences in elevation angle via transmit beamforming has been undertaken simultaneously on the same dataset recorded by a single receiver and that this cannot be achieved without the use of MIMO radar methods. See [9] for details and examples of our previous use of this algorithm in the MIMO radar context. While the remaining two modes preservation cases are not shown here we have been able to successively preserve each mode in turn and reject all other modes to the noise floor. Radar signals carried by certain "good" propagation modes can be isolated from all other "disturbed" modes and this can be done for every "good" mode simultaneously.

B. Range Dependent Beamforming

Geometric consideration of the propagation paths employed in OTHR mean that mode-selection/rejection beamformer solutions generated at one range may be ineffective for mode-rejection at different ranges. This is demonstrated in the following example in Fig. 10. Receiver data measured simultaneously at Elliott (1514km) and Tindal (1864km) has been processed as follows. Firstly, in Fig. 10(b), we have computed and applied a mode-selection/rejection beamformer to retain only the strongest mode at Tindal. Note that one mode remains and that the remaining two modes (location marked with white circles) have been rejected to the noise floor of the Doppler-range map. However, in Fig 10(c) we have applied this Tindal data generated beamformer to the shorter range Elliott data. From Fig. 10(c) it is clear that mode rejection for the rejected-at-Tindal mode is now poor.

Fig. 7. End aspect photograph showing the 12 element minimum redundancy array used in the Mode Selection Experiment. The total aperture length was 1200m and the array was oriented with end-fire at a bearing of 359.5^{o}T. The photo is taken from the southern end of the array looking north. The white equipment shelter just visible on the horizon contained the transmitter equipment and the central control system for the experiment. It was located mid-way along the array.

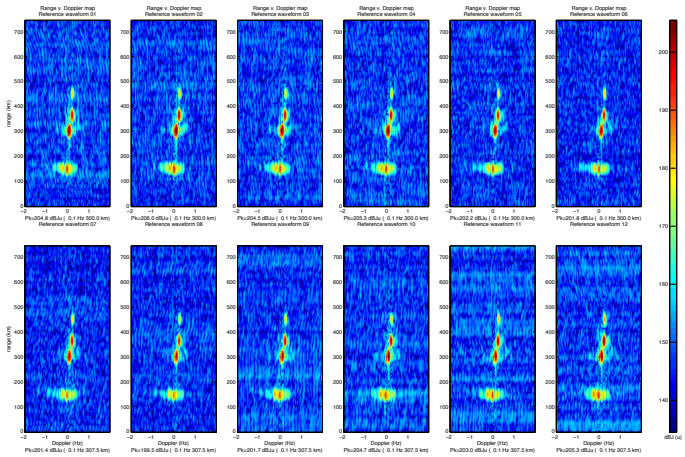

Fig. 8. Mt Everard received range-Doppler maps for the 12 TX channel waveform set. For each of the 12 Doppler-range maps the units are Doppler (Hz) on the horizontal axis and radar range (km) on the vertical axis. The range axis and intensity axis are uncalibrated.

C. Azimuthal Dependence

In the previous section we presented results demonstrating that a MVDR mode-selective beamformer solution computed for one range is ineffective at different ranges. We have also investigated the azimuthal dependancy of the MVDR mode-selective beamformer solution. As with the range varying case we are able to show that the mode-selective beamformer solution computed at one range and azimuth is ineffective when applied to data collected at comparable range but different azimuth.

Table I in section V lists the locations of down-range receiver sites used in the experiment. The three sites at Mt Everard, Hermannsburg, and Kings Canyon are of similar range but different azimuth. In fact this was the key criteria in selecting the sites. We have investigated all combinations of the MVDR mode-selective beamformer solution computed using data at one location and applied at that location and also applied to the remaining two locations. In all cases the mode-selective beamformer solution determined at a given location did not prove to be effective when applied to data received at the remaining locations, yet was highly effective as a mode selection beamformer for data at the same location.

We present one example showing the azimuthal dependency of the mode-selective beamformer solution in Fig. 11. These results are typical of all the cases examined.

In an example from dataset 10-001000 five modes propagated over the Coondambo to Kings Canyon path. The single waveform range-Doppler map is shown in Fig. 11(a). We have selected the 1E (first mode out in range) to preserve and our goal is to reject all other propagation modes. This was achieved at Kings Canyon using the MVDR mode-selective beamformer solution as shown in Fig. 11(b). All unwanted modes have been rejected to the level of the noise floor. The same beamformer solution applied to data received at Hermannsburg is ineffective and five propagation modes can clearly be seen in the range-Doppler map of Fig. 11(c). This poor rejection performance is caused by both a slightly different ionospheric structure on the Coondambo to Hermannsburg path compared with the Coondambo to Kings Canyon path and also the sidelobe properties of the transmit array. These factors are important in the radar backscatter case for spatially distributed clutter from the earth surface.

D. Beamformer Temporal Stability

The temporal stability of the mode rejection MVDR beamformer solution has been investigated. Fig 12 contrasts the mode rejectability of the $1F_{2l}$ mode for two cases using dataset 09-070200 recorded over the Mt Everard path. In the first (solid line) the $1F_{2l}$ mode is rejected continually through the 110s period shown. Mode rejectability of greater than 55dB is achieved for all coherent processing intervals (32s coherent interval and 10s processing stride). By contrast the dashed line shows rejectability for the case where the rejection beamformer solution is determined during the first coherent interval (32s) then held fixed and applied to every subsequent coherent processing interval (32s coherent interval and 10s processing stride). Rejectability drops quickly and is less than 40dB after 30s and less than 30dB after 110s.

This result is typical and demonstrates that the ionosphere is sufficiently dynamic that the mode rejection beamformer becomes “stale” and rejection performance deteriorates after short intervals.

E. Elevation Angle from Direction-of-Departure

Mode elevation take-off angle estimates determined using the MISO array exploit direction-of-departure estimates measured using the array and the known bearing from the transmitter array to the receiver locations. Elevation angles estimates determined from the OIS data are computed using the known ground range between OIS transmitter and receiver and the measured OIS range between transmitter and receiver and assume a spherical ionosphere.

The elevation take-off angle estimates determined using the MISO transmit array have been cross-checked with the same mode elevation take-off angles determined from the OIS data.

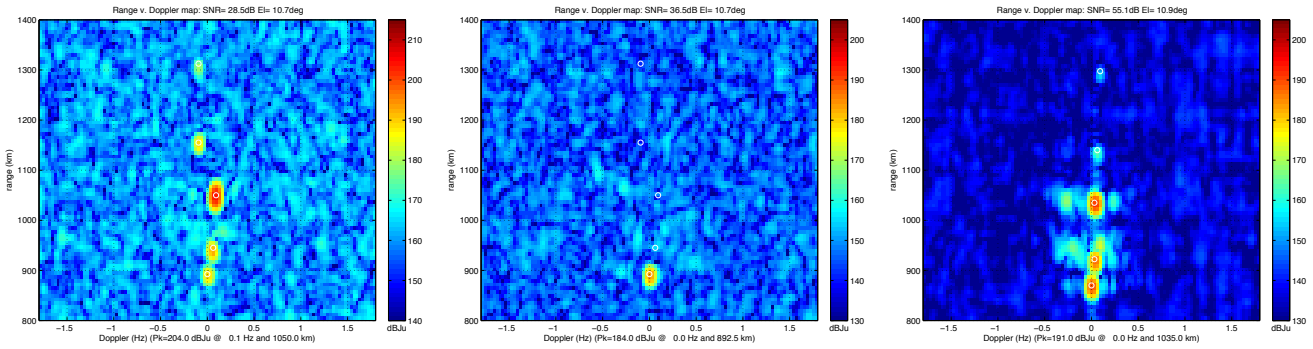

(a) Single Channel Response showing five modes (b) Preserve 1E mode at Kings Canyon (c) Kings Canyon weights at Hermannsburg

Fig. 11. A series of range-Doppler maps show the effect of the adaptive transmitter processing for different azimuths and similar range. The first subfigure corresponds to a single waveform channel showing the mode structure measured at Kings Canyon (range 867km azimuth -30.1^o). The second subfigure is the range-Doppler map showing the mode-selection/rejection beamformer determined using and applied to the Kings Canyon data. The third subfigure is the range-Doppler map showing the mode-selection/rejection beamformer determined using the Kings Canyon data but then applied to the simultaneously recorded Hermannsburg data (range 844.4km azimuth -21.3^o). Note the poor mode rejection of all modes. The noise levels were higher at Kings Canyon due to local effects nearby the receiver. In all three cases, the units are Doppler (Hz) on the horizontal axis and radar range (km) on the vertical axis, and the intensity units dBJu are dB Joules uncalibrated.

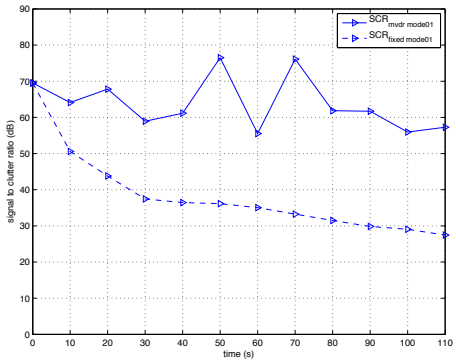

Fig. 12. Time evolving mode rejectability for the 1F$_{2l}$ mode for the case of a new rejection beamformer for each coherent processing interval (solid line) and the case of a fixed mode rejection beamformer where the beamformer solution is determined using only the first coherent processing interval (32s) of data.

Mode	Elev$_{DOD}$(^{o})	Elev$_{OIS}$(^{o})
1E	12.4	13.0
1F$_{2l}$	31.4	31.0
1F$_{2h\text{-}o}$	34.3	34.3
1F$_{2h\text{-}x}$	38.4	39.4

TABLE II

COMPARISON OF TAKE-OFF ELEVATION ANGLE ESTIMATES DETERMINED USING THE MISO TRANSMIT ARRAY AND OIS DATA FOR DATASET 09-070615.

Mode	Elev$_{DOD}$(^{o})	Elev$_{OIS}$(^{o})
1E	10.3	11.0
1F$_{2l}$	27.5	27.5
1F$_{2h\text{-}o}$	34.3	33.5
1F$_{2h\text{-}x}$	45.6	44.3

TABLE III

COMPARISON OF TAKE-OFF ELEVATION ANGLE ESTIMATES DETERMINED USING THE MISO TRANSMIT ARRAY AND OIS DATA FOR DATASET 10-012300.

Two example results are presented for the Mt Everard path. These results are typical of many such elevation angle measurement comparisons analysed. The first example corresponds to dataset 09-070615 recorded during MSE-I and is listed in table II while the second is from dataset 10-012300 recorded during MSE-II and is shown in table III. There is good agreement between the two different methods for determining elevation angle with root mean square difference between the two methods of less than 0.65^o and 0.95^o respectively. Note that the MISO architecture enables these estimates to be derived from data recorded by a single receiver.

F. Aperture Resolution

An estimate of the resolution of the Coondambo transmit array was obtained on the 1514km path to Elliott by opportunistically exploiting a period of ionospheric change. The elevation angle of any "high-ray" response versus the elevation angle of the response from "low ray" propagation for the same layer converges to a single elevation value at the maximum usable frequency (MUF) for a particular mode. This is because the high ray (1F$_{2h\text{-}x}$) and low ray (1F$_{2l}$) paths also converge into a single path. This feature of the ionosphere was exploited by leaving frequency of operation for the transmitter system fixed (f$_c$=9.26MHz) during a period where the MUF of ionosphere was higher than that frequency, but steadily diminishing (as measured using the co-located OIS system). Such a circumstance allowed for a steady progression from fully resolvable high-ray and low-ray (1F$_{2h\text{-}x}$ and 1F$_{2l}$) responses (separated by over 6^o in elevation) down to unresolvable mode responses (and then eventually no response as the MUF dipped below the operating frequency).

We examined the performance of the MVDR mode selective beamformer for the case of preserving the 1F$_{2l}$ while rejecting the 1F$_{2h\text{-}x}$ mode. Rejectability was high initially but decreased as the two modes became closer in elevation angle. As expected the adaptive beamformer performance became poor with the preserved mode signal to noise ratio rapidly decreasing as the resolution of the transmit array became

inadequate with the reducing mode elevation separation. We then designated the resolution limit as the elevation separation between the two modes such that the adaptive beamformer no longer enhanced the signal to noise ratio of the preserved mode. Using this approach the estimate of the resolution of the array was 4.8^o at a steer angle of 20^o. This compared favourably with a calculated Rayleigh limit of 4.5^o for the operating frequency f_c=9.26MHz and a projected aperture of (1200m at 20^o) of 410m.

G. Energy Budget Comparison

MIMO techniques reduce radar sensitivity proportionally to the waveform set cardinality M_t according to $P_{\text{MIMO}} = 10\log(M_t)$ where P_{MIMO} is the sensitivity penalty in dB. For the M_t=12 waveforms used in MSE then P_{MIMO}=10.8dB. For traditional surveillance radars this penalty can be recovered trading surveillance region scan time for extended coherent processing interval. This is generally not possible in OTHR. The penalty P_{MIMO} renders MIMO approaches unsuitable for OTHR target-detection-in-noise problems since target SNR will decrease by P_{MIMO} and detectability will decrease accordingly. In limited cases the target may be have excess SNR and the P_{MIMO} penalty may not be a concern.

In many cases encountered in OTHR, however, target detectability is limited by clutter of one form or another and not by noise. Clutter is unwanted return scatter from the radar transmission and for the target-in-clutter detectability case the clutter-to-noise ratio (CNR) scales the same as target SNR with reduced radar sensitivity. This means that target-to-clutter ratio (SCR) is unchanged with the reduced sensitivity of MIMO (at least until sensitivity is so reduced that the problem reverts to the target-in-noise case). MIMO is a useful approach for reducing clutter and hence in clutter limited cases it may improve target detectability in which case the penalty P_{MIMO} is of no concern.

During MSE we examined the energy budget of the one-way transmission system. In the example reported here we measured the SNR of a preserved mode (σ_{ps}=40dB) in the MISO case for a total transmitter power summed across all power amplifiers of P_{t}=378.5W. We then applied the computed beamformer weights at the transmitter location to form a conventional SISO transmit beam and re-measured the preserved mode SNR (σ_{ps}=43dB) and total transmitter power (P_{t}=61.8W). The relative sensitivity between the SISO and MISO cases is directly computed as

$$S_{\frac{\text{SISO}}{\text{MISO}}} = 10\log(378.5/61.8) + (43 - 40) = 10.87\text{dB} \quad (10)$$

which corresponds well with the expected relative sensitivity of P_{MIMO}=10.8dB

H. Mixed-Mode Correlation on Backscatter

Consider the two-way backscatter case comprising the Coondambo transmitter to Kings Canyon transponder to Glendambo receiver path. Assume mixed-mode propagation such as the simple two layer E-layer and F-layer situation where there are four possible two-way paths: E-E, F-F, E-F and F-E. Prior to the experiment we had conjectured that if the mixed modes (e.g. E-F and F-E) were correlated it may be possible to exploit the self-cancellation property of adaptive beamformers to remove both mixed modes using a beamformer at one of either the transmit or receive sites. A full treatment on self-cancellation in adaptive arrays is given in [47].

Assume we wish to preserve E-E propagation and reject all other two-way modes (F-F, E-F and F-E) using mode selectivity at only the transmit site. Assume all four modes are uncorrelated. In the two-layer example the E-E mode is preserved and the F-F and F-E modes are sufficiently different in direction-of-departure, for the aperture size, that they can be removed using the MVDR mode-selective beamformer. The E-F mode will have the same direction-of-departure as E-E so that suppression of E-F while preserving E-E will not be possible. In this case both E-E and E-F will remain and F-F and F-E will be removed.

If we now assume (our conjecture) that the F-E and E-F modes are correlated. The MVDR mode-selective beamformer will retain unit gain at the direction-of-departure angle of the desired mode E-E and form such gain in the beampattern in the direction-of-departure angle of the F-E and F-F modes as to suppress F-F and F-E and also coherently cancel the main-beam E-F mode with only the E-E mode remaining.

The implication of the conjecture being correct is profound as it would mean that both mixed modes could be suppressed at either the transmit or the receiver site alone and so a two dimensional aperture would be required at only one-of the transmit or receive sites.

Results from our investigation are shown in Fig. 13 where we have a typical two-layer return from the Kings Canyon transponder. In Fig. 13(a) the full range-Doppler map is shown. Earth return clutter is apparent surrounding zero Doppler (+/- 0.5Hz) from approximately 1600km (double-range) and corresponds to clutter from the ocean noting that since both the transmit and receive antenna have poor or no directive response the ocean clutter corresponds to scatter from ocean in any direction with respect to Coondambo. The direct-wave from Coondambo to Glendambo (15.8km) can be seen at zero Doppler and approximately 16km range. The band of spread-Doppler clutter appearing from 200km to 500km (two-way range) is due to scatter from meteors entering the ionosphere.

The transponder is visible at approximately -1.5Hz Doppler and from 1700km to 2200km (two-way range). To first order the three returns correspond to the four modes expected for a two-layer ionosphere noting the the two mixed-modes E-F and F-E appear together. An expanded view of the transponder return is shown in Fig. 13(b) where the modes are E-E, E-F and F-E, and finally F-F as range increases. Note that the mixed modes have slightly different range. The transponder is a single point scatterer on the surface of the earth. Longer propagation paths such as those via the higher altitude F-layer appear at longer range.

Fig. 13(c) shows the result of the MVDR mode-selective beamformer designed to preserve the E-E mode and reject the F-E and F-F modes (i.e. the training data cells comprised those cells that included the F-E and F-F modes in the range-Doppler map of Fig. 13(b)). The key result is that while the F-E and F-F modes are removed the E-E and the E-F remain. Including

F-E in the training data has failed to coherently cancel the E-F return. We examined all combinations of preserve direction (E-E, F-F and direct-wave) and training data selection (E-E, E-F, F-E, F-F and combinations) and were unable to create single E-E or F-F mode beamformer solutions. Either all modes were removed or two combinations remained. Our conjecture is incorrect and joint transmit and receive site mode-selectivity is required to remove mixed mode propagation.

I. Mode Selection on Receive

While the Mode Selection Experiment was concerned with demonstrating mode-selectivity on transmit we took the opportunity of the installed experimental equipment to confirm established results for mode-selectivity on receive [8]. When implementing mode-selectivity on receive one does not require a multiple waveform set on transmission so only a single waveform was transmitted from the Elliott transmitter. The mode-selectivity on receive case corresponds to the target to receiver part of the two-way OTHR situation.

For a limited period prior to the beginning of the MSE-II campaign the transmit system at Coondambo was replaced with a multi-channel receiver connected one channel per element to the 12 element minimum redundancy array. The down-range Elliott site was configured to transmit a single radar waveform which is shown in Fig. 6.

A representative example of the measured data is shown in Fig. 14 which shows the single channel received signal in Fig. 14(a) and the output of a MVDR mode-selective beamformer designed to retain the E-layer propagation mode in Fig. 14(b). All modes other than 1E are rejected to the system noise floor. The signal at a range of 1480km and Doppler offset of 1.5Hz was a local-to-the-receiver injected calibration signal and should be ignored.

The results comprehensively confirmed other authors claims that mode-selection on receive is achievable provided the receiver aperture is sufficient.

VII. Conclusion

This paper reports the first demonstration of mode selectivity on transmit for a one-way ionospherically propagated signal using an adaptive transmit array with sufficient aperture. We have shown using adaptivity on transmit that mode-selection/rejection can be achieved on representative ionospheric propagation paths by controlling the illumination. It is possible to preserve a chosen mode and reject all other modes and this can be applied for each mode simultaneously. Mode-selection beamformer solutions generated at one range are ineffective for mode-selection/rejection at different ranges. Effective mode-selection/rejection beamformer solutions need to be range dependent. Mode-selection beamformer solutions generated at one azimuth are ineffective for mode-selection/rejection at different azimuth but with comparable range. Effective mode-selection/rejection beamformer solutions vary with azimuth and interact with the sidelobe characteristic of the transmit antenna. This is an important issue in the case of distributed scatterer returns such as earth return clutter in OTHR.

The temporal stability of a particular mode-selection/rejection beamformer solution is poor and fixed mode-rejection beamformer solutions have reduced performance. Adaptive beamformer solutions are required for the radar signals at the time of transmission to sustain beamformer performance in the presence of the dynamic ionosphere. The mode take-off elevation angle determined using OIS data compares well with direction-of-departure estimates determined using the MISO transmit array. Measurement of the practical limit of aperture resolution for the array used agrees well with the directly calculated Rayleigh limit and the chosen aperture of 1200m has proven sufficient for mode-selection/rejection as required for a Mode Selective OTHR.

Demonstration of the energy budget penalty associated with MIMO is supported by a comparison of the respective MISO and SISO energy budgets. There is insufficient correlation between the E-F and F-E mixed modes to rely upon the coherent signal self-cancellation property of the MVDR beamformer to remove the mixed mode that has the same direction-of-departure as the preserved mode and hence apply mode-selectivity at only one of the transmit or receive sites. Minor reconfiguration of our test configuration allowed us to confirm previous results showing mode-selectivity on receive is achievable provided the array aperture is sufficient.

VIII. Acknowledgements

The ray-tracing plots published in this paper were obtained using the HF propagation toolbox, PHaRLAP, created by Dr Manuel Cervera, Defence Science and Technology Organisation, Australia (manuel.cervera@dsto.defence.gov.au). This toolbox is available by request from its author.

The authors thank the staff of HF Radar Branch, Intelligence, Surveillance and Reconnaisance Division of the Defence Science and Technology Organisation, Australia, for the custom equipment and the installation, operation and deconstruction of the experiment.

References

[1] M. I. Skolnik, *Radar Handbook*, 3rd ed. McGraw-Hill, 2008.

[2] G. Frazer, D. Meehan, Y. Abramovich, and B. Johnson, "Mode-Selective OTHR: A new cost-effective sensor for Maritime Domain Awareness," in *Radar Conference, 2010 IEEE*, May 2010, pp. 935–940.

[3] G. Frazer, B. Johnson, and Y. Abramovich, "Orthogonal waveform support in MIMO HF OTH radars," in *Waveform Diversity and Design Conference, 2007. International*, June 2007, pp. 423–427.

[4] Y. Abramovich, G. Frazer, and B. Johnson, "Noncausal adaptive spatial clutter mitigation in monostatic MIMO radar: Fundamental limitations," *Selected Topics in Signal Processing, IEEE Journal of*, vol. 4, no. 1, pp. 40–54, Feb. 2010.

[5] Y. Abramovich and G. Frazer, "Theoretical assessment of MIMO radar performance in the presence of discrete and distributed clutter," in *Signals, Systems and Computers, 2008 42nd Asilomar Conference on*, Oct. 2008, pp. 629–633.

[6] Y. Abramovich, G. Frazer, and B. Johnson, "Iterative adaptive Kronecker MIMO radar beamformer: Description and convergence analysis," *Signal Processing, IEEE Transactions on*, vol. 58, no. 7, pp. 3681–3691, July 2010.

[7] Y. Abramovich and G. Frazer, "Bounds on the volume and height distributions for the MIMO radar ambiguity function," *Signal Processing Letters, IEEE*, vol. 15, pp. 505–508, 2008.

[8] B. A. Johnson and Y. I. Abramovich, "Elevation filtering in wide-aperture HF skywave radar," in *Proceedings of the IEEE Radar Conference*, Boston, MA, USA, 17-20 April 2007, pp. 367–372.

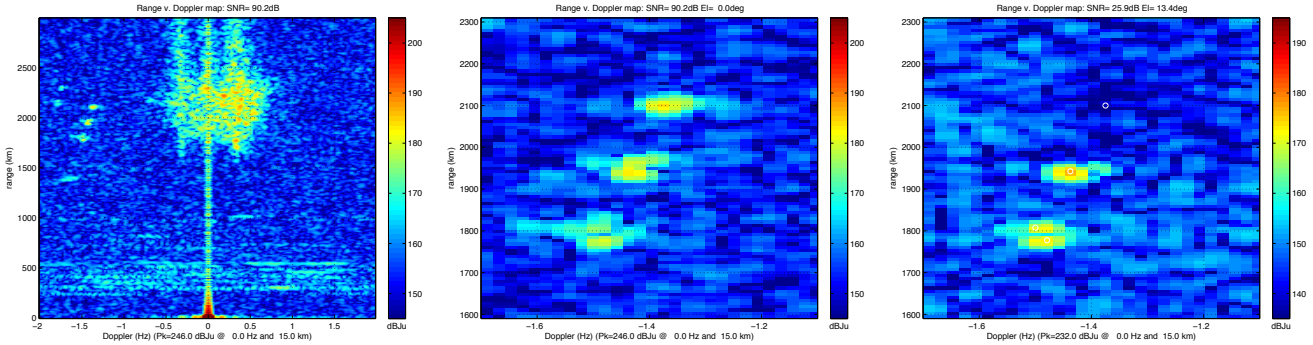

(a) Backscatter case measured at Glendambo (b) Expanded view showing transponder returns (c) Preserve E-E and reject F-E and F-F modes

Fig. 13. A series of range-Doppler maps show the two-way backscatter data for the Kings Canyon transponder return. The first sub-figure shows the full range-Doppler map comprising the direct signal from the transmitter at 16km range (two-way) and 0Hz Doppler, a band of direct scatter from meteors passing through the ionosphere at all Dopplers and the band of ranges from 200-500km (two-way), ocean clutter is apparent surrounding zero Doppler (+/- 0.5Hz) from approximately 1600km (double-range) and the transponder is visible at approximately -1.5Hz Doppler and from 1700km to 2200km (two-way range). The second sub-figure is an expanded view of the transponder return showing E-E, E-F, F-E and F-F returns over increasing range. The E-F and F-E returns are almost overlapping. The final sub-figure is one example of the MVDR mode-selective beamformer applied to the data. In this case the E-E mode is preserved and training data selected from F-E and F-F mode returns. E-E and E-F remain. Including F-E in the training data has failed to coherently cancel the E-F return. In all three cases, the units are Doppler (Hz) on the horizontal axis and radar range (km) on the vertical axis, and the intensity units dBJu are dB Joules uncalibrated.

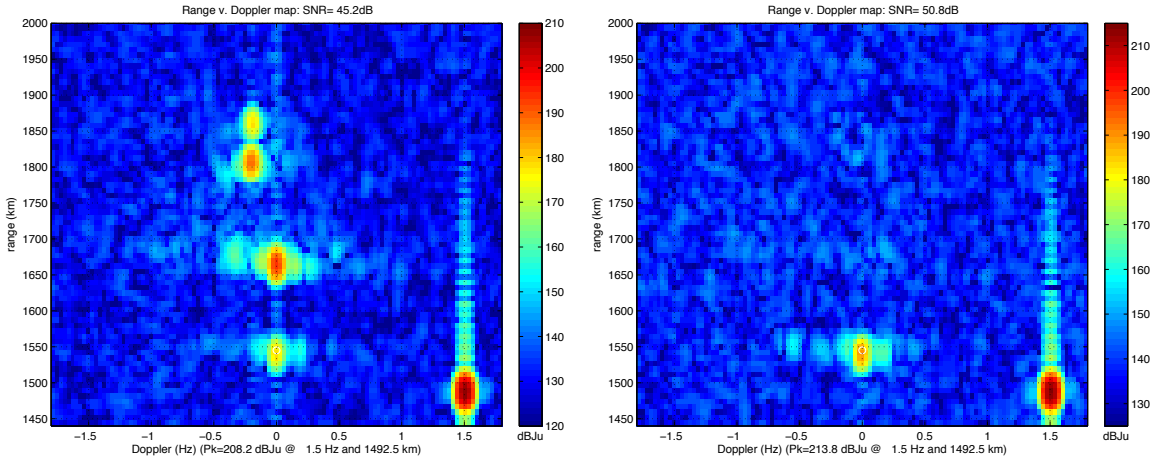

(a) Single Channel Response showing four modes (b) Preserve 1E mode transmitted from Elliott

Fig. 14. Range-Doppler maps showing the results of the mode-selection demonstration on receive experiment. Fig. 14(a) shows the single channel result with 1E, $1F_{2l}$, $1F_{2h\text{-}o}$ and $1F_{2h\text{-}x}$ propagation modes (ordered in increasing range) together with a local to the receiver injected calibration signal at 1.5Hz Doppler and 1480km range. Mode-selection was applied using the MVDR mode-selective beamformer with the 1E propagation preserved and all other modes rejected. This is shown in Fig. 14(b). In both cases, the units are Doppler (Hz) on the horizontal axis and radar range (km) on the vertical axis, and the intensity units dBJu are dB Joules uncalibrated.

[9] G. Frazer, Y. Abramovich, and B. Johnson, "Multiple-input multiple-output over-the-horizon radar: Experimental results," *Radar, Sonar Navigation, IET*, vol. 3, no. 4, pp. 290–303, August 2009.

[10] ——, "MIMO based spatial calibration of OTHR transmit arrays," in *Radar Conference - Surveillance for a Safer World, 2009. RADAR. International*, Oct. 2009, pp. 1–5.

[11] ——, "MIMO radar limitations in clutter," in *Radar Conference, 2009 IEEE*, May 2009, pp. 1–5.

[12] ——, "Mode-selective OTH radar: Experimental results for one-way transmission via the ionosphere," in *Radar Conference, 2011 IEEE*, May 2011, pp. 397–402.

[13] N. J. Willis, *Bistatic Radar*, 2nd ed. Technology Service Corporation, 1995.

[14] N. J. Willis and H. D. Griffiths, Eds., *Advances in Bistatic Radar*. SciTech Pub. Inc., 2007.

[15] C. J. Baker and H. D. Griffiths, *Advances in Sensing with Security Applications*. Springer, 2006, ch. 1, pp. 1–22.

[16] M. Cherniakov, Ed., *Bistatic Radar: Principles and Practice*. Wiley, 2007.

[17] S. Kingsley and S. Quegan, *Understanding Radar Systems*. SciTech, 1999, chapter 13.

[18] V. S. Chernyak, *Fundamentals of Multisite Radar Systems: Multistatic Radars and Multistatic Radar Systems*. CRC, 1998.

[19] J. Li and P. Stoica, *MIMO Radar Signal Processing*. Wiley-IEEE Press, 2008.

[20] M. Wicks, E. L. Mokole, S. Blunt, R. Schneible, and V. Amuso, Eds., *Principles of Waveform Diversity and Design*. SciTech Publishing, 2010.

[21] J. R. Guerci, *Cognitive Radar: The Knowledge-Aided Fully Adaptive Approach*. Boston, USA: Artech House, 2010.

[22] J. Dorey and G. Garnier, "The RIAS pulsed synthetic-antenna radar," *L'Onde Electrique*, vol. 69, pp. 36–44, 1989.

[23] A.-S. Luce, H. Molina, D. Muller, and V. Thirard, "Experimental results on RIAS digital beamforming radar," in *Radar 92. International Conference*, Oct. 1992, pp. 74–77.

[24] R. Hoctor and S. Kassam, "The unifying role of the coarray in aperture synthesis for coherent and incoherent imaging," *Proceedings of the IEEE*, vol. 78, no. 4, pp. 735–752, April 1990.

[25] A. Haimovich, E. Fishler, R. Blum, L. Cimini, D. Chizhik, and R. Valenzuela, "Statistical MIMO radar," in *Proceedings ASAP Workshop*. MIT-

LL, 2003.
[26] K. Forsythe, D. Bliss, and G. Fawcett, "Multiple-input multiple-output (mimo) radar: Performance issues," in *Proc. 38th Asilomar Conference on Signals, Systems and Computers*, vol. 1. Pacific Grove, CA, USA: IEEE, Nov 7-10 2004, pp. 310–315.
[27] F. Robey, S. Coutts, D. Weikle, J. McHarg, and K. Cuomo, "MIMO radar theory and experimental results," in *Signals, Systems and Computers, 2004. Conference Record of the Thirty-Eighth Asilomar Conference on*, vol. 1, Nov. 2004, pp. 300–304 Vol.1.
[28] S. Coutts, K. Cuomo, J. McHarg, F. Robey, and D. Weikle, "Distributed coherent aperture measurements for next generation BMD radar," in *Sensor Array and Multichannel Processing, 2006. Fourth IEEE Workshop on*, July 2006, pp. 390–393.
[29] G. Frazer, Y. Abramovich, B. Johnson, and F. Robey, "Recent results in MIMO over-the-horizon radar," in *Radar Conference, 2008. RADAR '08. IEEE*, May 2008, pp. 1–6.
[30] F. Robey and S. Coutts, "MIMO techniques applied to OTHR," 2010, private correspondence.
[31] J. Kantor and S. Davis, "Airborne GMTI using MIMO techniques," in *Radar Conference, 2010 IEEE*, May 2010, pp. 1344–1349.
[32] J. Kantor and D. Bliss, "Clutter covariance matrices for GMTI MIMO radar," in *Signals, Systems and Computers (ASILOMAR), 2010 Conference Record of the Forty Fourth Asilomar Conference on*, Nov. 2010, pp. 1821–1826.
[33] V. Mecca and J. Krolik, "MIMO STAP clutter mitigation performance demonstration using acoustic arrays," in *Signals, Systems and Computers, 2008 42nd Asilomar Conference on*, Oct. 2008, pp. 634–638.
[34] J. Yu and J. Krolik, "Quadrature slow-time MIMO radar with experimental results," in *Signals, Systems and Computers (ASILOMAR), 2010 Conference Record of the Forty Fourth Asilomar Conference on*, Nov. 2010, pp. 2134–2137.
[35] V. Mecca and J. Krolik, "MIMO enabled multipath clutter rank estimation," in *Radar Conference, 2009 IEEE*, May 2009, pp. 1–6.
[36] R. Riddolls, M. Ravan, and R. Adve, "Canadian HF over-the-horizon radar experiments using MIMO techniques to control auroral clutter," in *Radar Conference, 2010 IEEE*, May 2010, pp. 718–723.
[37] R. Riddolls, "Joint transmit-receive adaptive beamforming experimental results from an Auroral-zone Canadian over-the-horizon radar system," in *Radar Conference, 2011 IEEE*, May 2011, pp. 548–553.
[38] J. Barnum, "Ship detection with high-resolution HF skywave radar," *Oceanic Engineering, IEEE Journal of*, vol. 11, no. 2, pp. 196–209, Apr 1986.
[39] R. Barnes, "Automated propagation advice for OTHR ship detection," *Radar, Sonar and Navigation, IEE Proceedings* -, vol. 143, no. 1, pp. 53–63, Feb 1996.
[40] K. Davies, *Ionospheric Radio*. Peter Peregrinus, 1990.
[41] M. Turley and M. Tyler, "A technique for estimating the detection performance of a skywave over-the-horizon radar," in *Proceedings of the IEEE International Radar Conference*. Bordeaux, France: SEE, 12-16 October 2009.
[42] A. Cameron, "The Jindalee Operational Radar Network: Its architecture and surveillance capability," in *Proceedings of the IEEE International Radar Conference*, 1995, pp. 692–697.
[43] V. Bazin, J. Molinie, J. Munoz, P. Dorey, S. Saillant, G. Auffray, V. Rannou, and M. Lesturgie, "A general presentation about the OTH-R Nostradamus," in *Proceedings of the IEEE Radar Conference*, April 2006.
[44] J. Capon, "High resolution frequency-wavenumber spectrum analysis," *Proceedings of the IEEE*, vol. 57, no. 8, pp. 1408–18, Aug 1969.
[45] I. S. Reed, J. D. Mallett, and L. E. Brennan, "Rapid convergence rate in adaptive arrays," *IEEE Transactions on Aerospace and Electronic Systems*, vol. AES-10, pp. 853–863, 1974.
[46] J. M. Goodman and M. Daehler, "Use of oblique-incidence-sounders in HF frequency management," in *Proc. International Conference on HF Radio Systems and Techniques*. London, UK: IEE, 1988.
[47] B. Widrow, K. M. Duvall, R. P. Gooch, and W. C. Newman, "Signal cancellation phenomena in adaptive antennas: Causes and cures," *Antennas and Propagation, IEEE Transactions on*, vol. 30, no. 3, pp. 469–478, May 1982.